

An EL-model based passivity control of four-phase interleaved PFC

LI HUA-WU, MA HONG-XING, JIANG JIAN-FENG, YANG XI-JUN, YANG XING-HUA

*Key Laboratory of Control of Power Transmission and Conversion, Ministry of Education
Department of Electrical Engineering, Shanghai Jiao Tong University
800 Dongchuan RD. Minhang District, Shanghai, 200240 China*

e-mail: lihuawushui@163.com

(Received: 15.02.2012, revised: 30.08.2013)

Abstract: With the continuous increase of output power ratings, multi-phase (multi-channel) interleaved power factor corrector (IPFC) is gradually employed in domestic and commercial inverter air-conditioners. IPFC can solve several main problems, such as power rating increase, power device selection, input current ripple reduction as well as inductor on-board mounting. But for a multi-phase IPFC, the key problem is that it should show rapid dynamic responds and good current sharing capability, so in this paper the aim is to improve the dynamic performance and current sharing capability by means of passivity control theory. Considering the power circuit topology of a four-phase IPFC, an EL (Euler-Lagrange) mathematical model is established when the IPFC operates in continuous conduction mode (CCM). Then the passivity of the four-phase IPFC is proved, and the passivity-based controller using the state variables feedback and damping injection method is designed. The proposed control scheme, which is easy to control and needs no proportion integral controller, has strong robustness on disturbance from single-phase AC input voltage, the load as well as the parameters of the employed devices. Even in wide-range load condition, the mains current has a fast dynamic response and the average output voltage almost keep unchanged. As a result, the main functions of the four-phase IPFC are implemented including nearly unitary power factor and constant DC output voltage. Meanwhile, the four-phase IPFC acquires an excellent current sharing effect after using passivity-based controller. The above analysis has been proved with simulated results by means of MATLAB/SIMULINK and experimental results, showing that the passivity-based IPFC controller has superior performances and feasibility.

Key words: four-phase interleaved PFC, passivity-based control, damping injection, current sharing

1. Introduction

Single-phase active power factor corrector (PFC) has many advantages, such as lower harmonic currents and unitary power factor at mains side, constant DC output voltage at output side and simple circuit topology. It can achieve the “Green Conversion” of electrical power. In order to meet the requirements of large power applications, simplify the heat dissipation design and facilitate the selection of power switches and boost inductors, it is necessary to employ multi-phase interleaved structure for the design of high power PFC. The conventional

single channel PFC and IPFC are usually controlled using the traditional linear control theories [1-3] by sampling the instantaneous value of inductor currents and DC output voltage, but the control performance is not so ideal in case that the load changes in a large range due to the slower current response and the unsatisfactory dynamic performance when linear control strategies are utilized. According to its own switching characteristics, single channel PFC and IPFC are periodic time-varying systems. It is necessary to introduce advanced nonlinear control strategies to get better PFC control performance.

As one of the nonlinear control methods, the sliding model variable structure control [4-6] scheme has strong robustness against parameter variation and external disturbance and has better dynamic response, however in considering of its own control intrinsic feature, state variables will jitter when the system enters sliding model switching area, which will weaken the system performance. Passivity-based control is essentially the control of energy, which has been utilized in the many control fields, such as the controlled rectifiers [7-8], DC-DC converters [9-11], active power filters [12-19], and it can bring about good control effects on power electronic converters. When used in the design of controller, it can make the energy function accelerate convergence to the expected energy function under the precondition of system stability by properly injecting damping. In addition, for applications where single-phase active PFCs ought to output large power, for instance, variable-frequency cabinet air-conditioner applications, multi-phase parallel-connected interleaved structure has to be considered in order to improve the whole performance and reduce the total cost. Nevertheless, the problem of current sharing appears which imposes restrictions on the development of multi-phase IPFC. Taking all the above factors, the four-phase (four-stage or four-channel) IPFC is chosen as the object of study in the paper, and a passive controller is correspondingly designed by means of state feedback and damping injection on the basis of analysis of the EL mathematical model, which can lead to several advantages for IPFC, including fast current response, stable DC output voltage, good current sharing and strong capability against load disturbance, etc.

After the aforesaid introduction to the necessity of passivity control for high power multi-phase active IPFC, the contents to be explained in sequence are the establishment of EL model of IPFC in Section 1, the design of passivity-based IPFC controller in Section 2, the simulation analysis in section 3 and the experiment analysis in Section 4.

2. Establishment of EL model for IPFC

The power circuit topology of the four-phase IPFC is shown in Figure 1, where R_1 , R_2 , R_3 and R_4 stand for the equivalent series resistances of inductor L_1 , L_2 , L_3 and L_4 respectively. R_{s1} , R_{s2} , R_{s3} and R_{s4} stand for the equivalent on-resistances of IGBT S_1 , S_2 , S_3 and S_4 respectively. FRD₁, FRD₂, FRD₃ and FRD₄ are all fast recovery diodes. R_C is the equivalent series resistance of the output filter electrolysis capacitor C_2 , D_1 , D_2 , D_3 and D_4 are all commonly used diodes, which constitute a single-phase uncontrolled rectifier. C_1 denotes AC filter capacitor. R_o denotes the load. The devices with the same subscript constitute one phase PFC, including an inductor, an IGBT and a fast recovery diode. Supposing all the four inductors operate always in a linear state, and considering no inductor saturation.

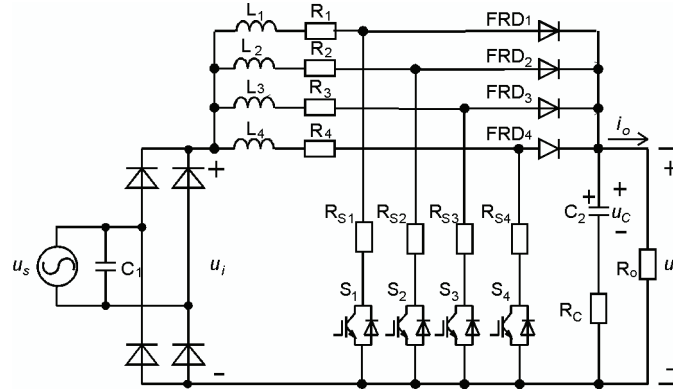


Fig. 1. Power circuit of the typical four-phase IPFC

Define S_i ($i = 1, 2, 3$ and 4) as the binary logic switching function of each switch. $S_i = 1$ means the i^{th} switch is in on state, and $S_i = 0$ means the i^{th} switch is in off state. Choosing inductor currents i_{L1} , i_{L2} , i_{L3} , i_{L4} and output electrolysis capacitor voltage u_c as the system state variables, according to Figure 1, the state space equation of the four-phase IPFC can be written as follows:

$$\begin{cases} L_1 \frac{di_1}{dt} = u_i - (R_1 + R_{s1} S_1) i_1 - (1 - S_1) U_o \\ L_2 \frac{di_2}{dt} = u_i - (R_2 + R_{s2} S_2) i_2 - (1 - S_2) U_o \\ L_3 \frac{di_3}{dt} = u_i - (R_3 + R_{s3} S_3) i_3 - (1 - S_3) U_o \\ L_4 \frac{di_4}{dt} = u_i - (R_4 + R_{s4} S_4) i_4 - (1 - S_4) U_o \\ C_o \frac{du_c}{dt} = (1 - S_1) i_1 + (1 - S_2) i_2 + (1 - S_3) i_3 + (1 - S_4) i_4 - \frac{U_o}{R_o}, \end{cases} \quad (1)$$

where u_i is the rectified single-phase AC voltage, namely the absolute value of AC input voltage. Equation 1 can be rewritten in EL (Euler-Lagrange) form as follows:

$$\mathbf{M}\dot{\mathbf{x}} + \mathbf{C}\mathbf{x} + \mathbf{R}\mathbf{x} = \mathbf{u}, \quad (2)$$

where \mathbf{M} is the positive definite diagonal matrix, and \mathbf{C} is the anti-symmetric matrix, ($\mathbf{C} = -\mathbf{C}^T$) which reflects the system internal interconnection structure; \mathbf{R} is the system dissipation element matrix, which reflects the system dissipation characteristics; \mathbf{u} is the system external input vector, and \mathbf{x} is the system state variable vector.

The detailed expressions of these matrices are listed as follows:

$$\mathbf{M} = \begin{bmatrix} L_1 & 0 & 0 & 0 & 0 \\ 0 & L_2 & 0 & 0 & 0 \\ 0 & 0 & L_3 & 0 & 0 \\ 0 & 0 & 0 & L_4 & 0 \\ 0 & 0 & 0 & 0 & C_o \end{bmatrix}, \quad (3)$$

$$\mathbf{C} = \frac{R_o}{R_o + R_C} \begin{bmatrix} 0 & 0 & 0 & 0 & (1-S_1) \\ 0 & 0 & 0 & 0 & (1-S_2) \\ 0 & 0 & 0 & 0 & (1-S_3) \\ 0 & 0 & 0 & 0 & (1-S_4) \\ -(1-S_1) & -(1-S_2) & -(1-S_3) & -(1-S_4) & 0 \end{bmatrix}, \quad (4)$$

$$\mathbf{R} = \begin{bmatrix} \phi_1 & 0 & 0 & 0 & 0 \\ 0 & \phi_2 & 0 & 0 & 0 \\ 0 & 0 & \phi_3 & 0 & 0 \\ 0 & 0 & 0 & \phi_4 & 0 \\ 0 & 0 & 0 & 0 & \frac{1}{R_o + R_C} \end{bmatrix}. \quad (5)$$

$$\phi_i = R_i + R_{S_i} S_i + \frac{R_o R_C (1-S_i)}{R_o + R_C} \quad (i = 1, 2, 3, 4), \quad (6)$$

$$\mathbf{u} = [u_i \quad u_i \quad u_i \quad u_i \quad 0]^T, \quad (7)$$

$$\mathbf{x} = [i_1 \quad i_2 \quad i_3 \quad i_4 \quad u_C]^T \quad (8)$$

3. Design of the passivity based IPFC

3.1. Proof of IPFC system passivity

Considering a nonlinear system S:

$$S: \begin{cases} \dot{\mathbf{x}} = \mathbf{f}(\mathbf{x}) + \mathbf{g}(\mathbf{x})\mathbf{u} \\ \mathbf{y} = \mathbf{h}(\mathbf{x}) \end{cases} \quad (9)$$

where $x \in R^n$ and $u \in R^m$ are the input vectors, $y \in R^m$ is the output vector. For $\forall t > 0$, if there is a positive semi-definite energy storage function $H(x)$ and a positive definite function $Q(x)$ that satisfy the dissipated inequality

$$\dot{H} \leq \mathbf{u}^T \mathbf{y} - Q(\mathbf{x}), \quad (10)$$

where $\mathbf{u}^T \mathbf{y}$ is the system energy supply rate. The system is strictly passive. The dissipated

inequality shows that the passive system is always operating with energy loss. Therefore, if there is a smoothly differentiable positive energy storage function $H(x)$, Equation is stable at the origin, and the storage function can be regarded as Lyapunov function [20].

The system handled in the paper is a four-phase IPFC. Considering a strictly passive system is still a strictly passive system after connected in-parallel or interleaved with others, it only needs to verify that the single-phase PFC is a strictly passive system.

Let the system energy function as $\mathbf{H} = \mathbf{x}^T \mathbf{M} \mathbf{x} / 2$, and $\dot{\mathbf{H}} = \mathbf{x}^T \mathbf{M} \dot{\mathbf{x}} = \mathbf{x}^T \mathbf{u} - \mathbf{x}^T \mathbf{R} \mathbf{x}$. Let $\mathbf{y} = \mathbf{x}$, $\mathbf{Q}(x) = \mathbf{x}^T \mathbf{R} \mathbf{x}$, evidently, the four-phase IPFC system is also strictly passive.

3.2. Determination of stable equilibrium point

When a four-phase IPFC operates in a steady state, it can bring about unitary input power factor and constant DC output voltage U_{DC} . According to the steady operation property of the boost type AC-DC converter, the four-phase IPFC steady function can be obtained as follows:

$$\begin{cases} I_s^* = \frac{U_s}{(1-d)^2 R_o} \\ U_o^* = \frac{U_s}{1-d}, \end{cases} \quad (11)$$

where d represents the duty ratio, I_s^* and U_o^* are the average input current and output voltage of the AC-DC converter respectively when operating around equilibrium point.

Given input current is I_s^* , then

$$I_s^* = \frac{U_o^{*2}}{U_s R_o}. \quad (12)$$

It can be derived from Equation 12 that the output voltage can keep constant by regulating the given input current around the equilibrium point. So the expected stable equilibrium system point is given as follows:

$$\begin{aligned} x_1^* &= x_2^* = x_3^* = x_4^* = \\ &= \frac{1}{4} I_s^* |\sin \omega_i t| = \frac{U_o^{*2}}{4 U_s R} |\sin \omega_i t| \end{aligned} \quad (13)$$

$$x_5^* = U_{DC}, \quad (14)$$

where ω_i represents the angular frequency of the single phase AC mains.

3.2.1. Design of passivity-based controller

The fundamental concept of passivity-based controller is to analyze the system matrix structure and find out the “reactive term”, which is corresponding to matrix C of the system by using the system Euler-Lagrange equation. It can be utilized to simplify the design of system controller, because it does not make any contributions to the control system or produce any power consumption. On the other hand, it can force the system energy function to track the expected energy function and make the system output error converge to zero gradually by injecting

damping term. The state feedback control law is designed to make \mathbf{x} track the expected value \mathbf{x}^* . Let $\mathbf{x}_e = \mathbf{x}^* - \mathbf{x}$ and choose the system error energy storage function as follows:

$$\mathbf{H}_e = \frac{1}{2} \mathbf{x}_e^T \mathbf{M} \mathbf{x}_e. \quad (15)$$

In order to make the system converge at the expected point and make the error energy function converge to zero quickly, it needs to inject damping to accelerate the system energy dissipation. At the same time, in order to achieve the decoupling control of dynamic and static performance, the following method is used for the design.

Let $\mathbf{R}_d \mathbf{x}_e = (\mathbf{R} + \mathbf{R}_a) \mathbf{x}_e$, where \mathbf{R}_a is the injected damping positive matrix. So Equation 2 can be transformed into

$$\begin{aligned} \mathbf{M} \dot{\mathbf{x}}_e + \mathbf{R}_d \mathbf{x}_e = \\ \mathbf{u} - [\mathbf{M} \dot{\mathbf{x}}^* + \mathbf{C}(\mathbf{x}^* + \mathbf{x}_e) + \mathbf{R} \mathbf{x}^* - \mathbf{R}_a \mathbf{x}_e]. \end{aligned} \quad (16)$$

Choose the control law as:

$$\mathbf{u} = \mathbf{M} \dot{\mathbf{x}}^* + \mathbf{C} \mathbf{x} + \mathbf{R} \mathbf{x}^* - \mathbf{R}_a \mathbf{x}_e. \quad (17)$$

Then, the above Control law makes

$$\dot{\mathbf{H}}_e = -\mathbf{x}_e^T (\mathbf{R} + \mathbf{R}_a) \mathbf{x}_e < 0. \quad (18)$$

Substituting Equation 2 for Equation (10) can obtain

$$\begin{aligned} \begin{bmatrix} u_i \\ u_i \\ u_i \\ u_i \\ 0 \end{bmatrix} &= \begin{bmatrix} L_1 & 0 & 0 & 0 & 0 \\ 0 & L_2 & 0 & 0 & 0 \\ 0 & 0 & L_3 & 0 & 0 \\ 0 & 0 & 0 & L_4 & 0 \\ 0 & 0 & 0 & 0 & C \end{bmatrix} \begin{bmatrix} \dot{x}_1^* \\ \dot{x}_2^* \\ \dot{x}_3^* \\ \dot{x}_4^* \\ \dot{x}_5^* \end{bmatrix} + \\ &+ \frac{R}{R+R_C} \begin{bmatrix} 0 & 0 & 0 & 0 & (1-S_1) \\ 0 & 0 & 0 & 0 & (1-S_2) \\ 0 & 0 & 0 & 0 & (1-S_3) \\ 0 & 0 & 0 & 0 & (1-S_4) \\ -(1-S_1) & -(1-S_2) & -(1-S_3) & -(1-S_4) & 0 \end{bmatrix} \begin{bmatrix} x_1 \\ x_2 \\ x_3 \\ x_4 \\ x_5 \end{bmatrix} + \\ &+ \begin{bmatrix} \phi_1 & 0 & 0 & 0 & 0 \\ 0 & \phi_2 & 0 & 0 & 0 \\ 0 & 0 & \phi_3 & 0 & 0 \\ 0 & 0 & 0 & \phi_4 & 0 \\ 0 & 0 & 0 & 0 & \frac{1}{R+R_C} \end{bmatrix} \begin{bmatrix} x_1^* \\ x_2^* \\ x_3^* \\ x_4^* \\ x_5^* \end{bmatrix} + \begin{bmatrix} R_{a1} & 0 & 0 & 0 & 0 \\ 0 & R_{a2} & 0 & 0 & 0 \\ 0 & 0 & R_{a3} & 0 & 0 \\ 0 & 0 & 0 & R_{a4} & 0 \\ 0 & 0 & 0 & 0 & R_{a5} \end{bmatrix} \begin{bmatrix} x_1 - x_1^* \\ x_2 - x_2^* \\ x_3 - x_3^* \\ x_4 - x_4^* \\ x_5 - x_5^* \end{bmatrix} \end{aligned} \quad (19)$$

According to the above control law, the switching function expressions of the four switches can be obtained as follows:

$$\left\{ \begin{array}{l}
 S_1 = \frac{u_i - L_1 \dot{x}_1^* - (R_1 + \frac{R_o R_C}{R_o + R_C})x_1^* + R_{a1}x_{1e} - \frac{R_o x_5}{R_o + R_C}}{R_{s1}x_1^* - (R_o x_5 + R_o R_C x_1^*) / (R_o + R_C)} \\
 S_2 = \frac{u_i - L_2 \dot{x}_2^* - (R_2 + \frac{R_o R_C}{R_o + R_C})x_2^* + R_{a2}x_{2e} - \frac{R_o x_5}{R_o + R_C}}{R_{s2}x_2^* - (R_o x_5 + R_o R_C x_2^*) / (R_o + R_C)} \\
 S_3 = \frac{u_i - L_3 \dot{x}_3^* - (R_3 + \frac{R_o R_C}{R_o + R_C})x_3^* + R_{a3}x_{3e} - \frac{R_o x_5}{R_o + R_C}}{R_{s3}x_3^* - (R_o x_5 + R_o R_C x_3^*) / (R_o + R_C)} \\
 S_4 = \frac{u_i - L_4 \dot{x}_4^* - (R_4 + \frac{R_o R_C}{R_o + R_C})x_4^* + R_{a4}x_{4e} - \frac{R_o x_5}{R_o + R_C}}{R_{s4}x_4^* - (R_o x_5 + R_o R_C x_4^*) / (R_o + R_C)}
 \end{array} \right. \quad (20)$$

3.3. Design of on-line load identification observer

It can be known from the above analysis that passive controller needs to know the load conditions to implement control. For the load applications with remarkable disturbance, the on-line identification load observer is designed to enhance the system robustness and further to make the system obtain good dynamic and static performances even at the disturbance of 50% rated load.

The mathematical model of the observer is written as follows:

$$R_o = \begin{cases} U_o / I_o & \frac{2}{3}R_r \leq U_o / I_o \\ \frac{2}{3}R_r & \frac{2}{3}R_r > U_o / I_o \end{cases}, \quad (21)$$

where R_r refers to the rated load resistance, U_o refers to the average DC output voltage, and I_o refers to the load current.

4. Simulation analysis

In order to prove the presented control strategy, the four-phase IPFC is simulated by means of MATLAB/SIMULINK, which is powered by the standard single phase AC sinusoidal voltage at 220 V/50 Hz. The passivity-based control system block diagram of one phase PFC within the four-phase IPFC is shown in Figure 2, and the control system for the four-phase IPFC is shown in Figure 3.

The other simulation conditions are listed below: the expected average DC output voltage 385 V, the rated output power 8.0 kW, each boost inductance 0.5 mH, the equivalent series resistance of each inductor 0.1 Ω , the total DC electrolysis capacitance $6 \times 680 \mu\text{F}$, the equivalent series resistance of each electrolysis capacitor 0.2 Ω , the conduction resistance of each IGBT 0.1 Ω , and switching frequency 35 kHz.

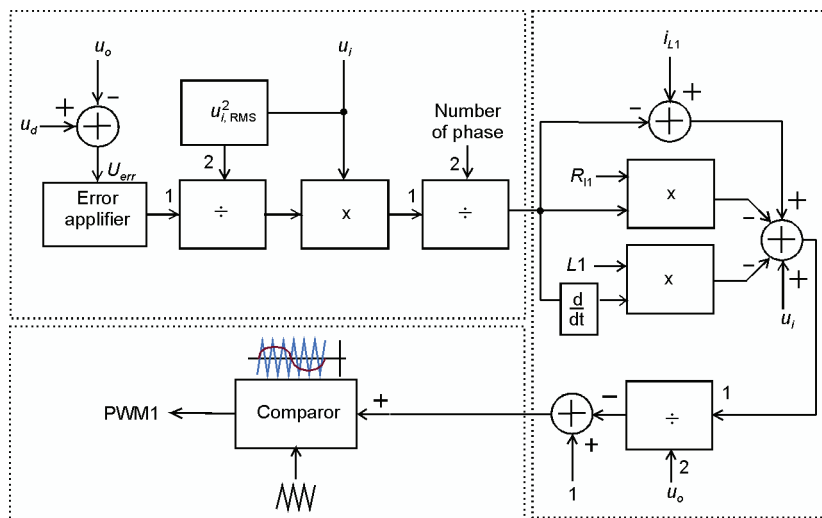


Fig. 2. Passivity control system block diagram for one phase PFC

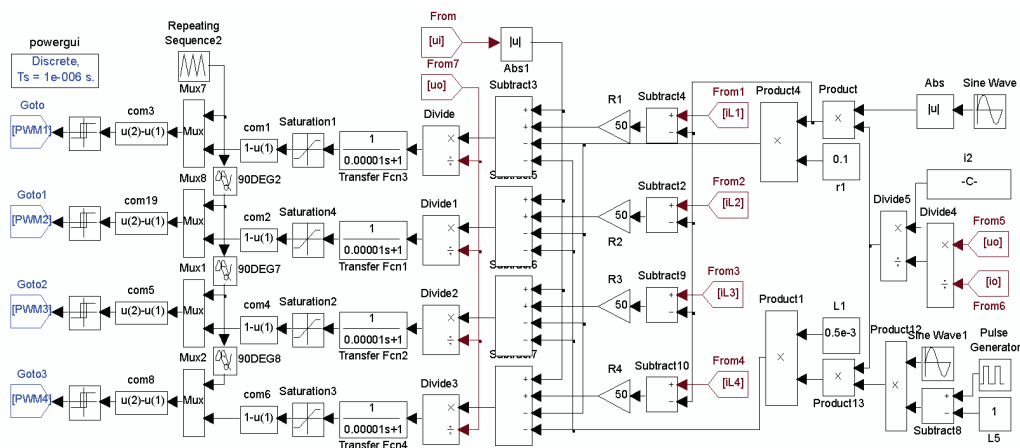


Fig. 3. Passivity control system simulation block diagram for the four-phase IPFC

Let the damping injection resistance $R_{a1} = R_{a2} = R_{a3} = R_{a4} = 40 \Omega$, then the mains voltage and mains current waveforms of the four-phase IPFC are shown in Figure 4. It can be seen easily that the mains current is strictly in phase with the mains voltage, which shows unitary power factor. The THD of mains current is only 2.33%. Points A, B and C refer to the

times when the duty ratio is 0.75, 0.5 and 0.25 respectively, where the summed inductor current ripple is near zero, which can be seen clearly in the partially enlarged square window. There are totally six such points within half a mains period. In addition, the mains current responds very fast due to the direct current control regardless of the change of mains voltage and the load.

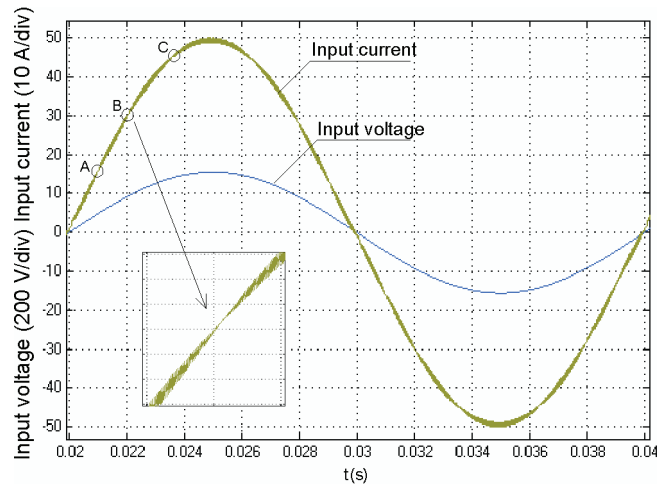


Fig. 4. Waveforms of mains voltage and mains current at the load of 7.8 kW

The DC output voltage also shows a very fast response. During startup phase at rated load, the needed time is about 0.2 s from zero to 95% of the expected DC output voltage. In steady state, the waveform of DC output voltage is shown in Figure 5. Obviously, the average DC output voltage is 385 V with the maximum peak to peak value of the DC ripple voltage of about 10 V.

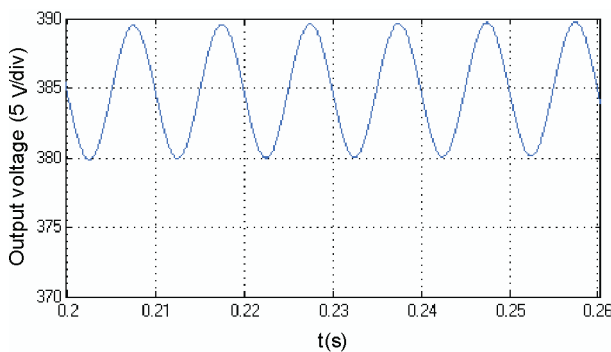


Fig. 5. Waveform of the DC output voltage at the load of 7.8 kW

It is well known that the four-phase IPFC can simplify the design of boost inductors and reduce the mains current ripple, but in practice, the parameter difference among different phase PFCs can cause the unbalanced currents, which will make the whole power circuit

malfunction. Parameter deviation includes inductance, inductor's ESR, capacitor's ESR as well as conduction resistance of power switches.

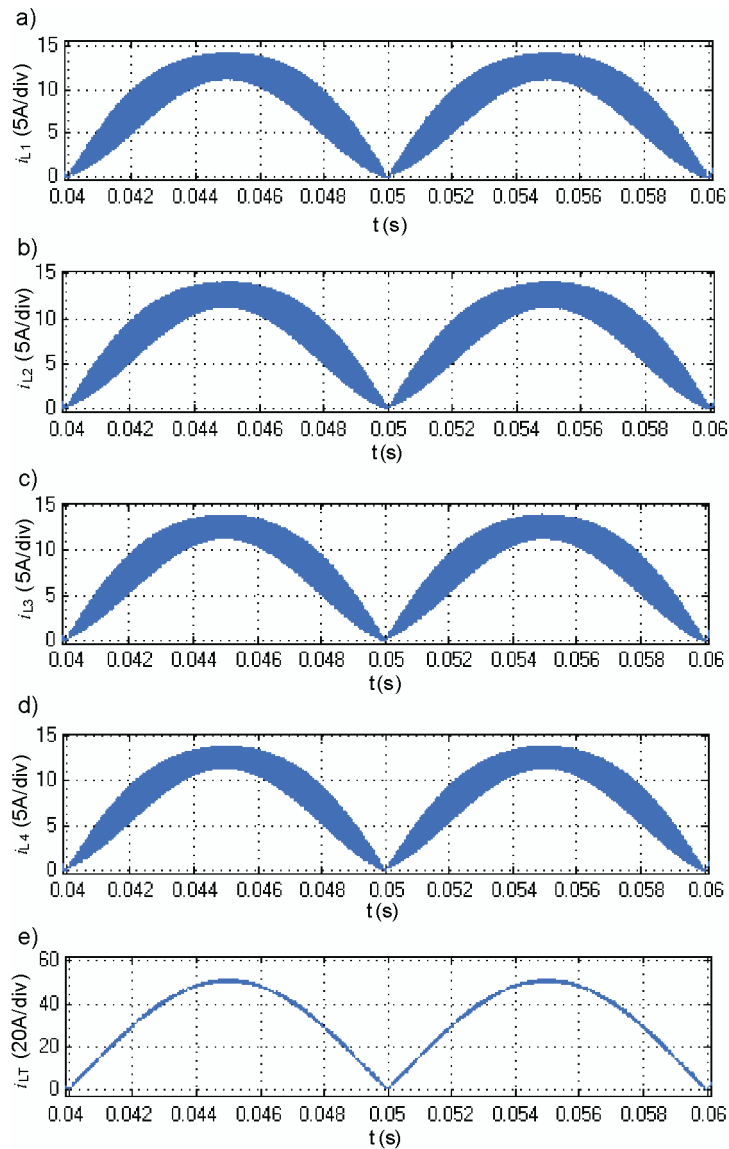


Fig. 6. Waveforms of current for the four-phase IPFC: a) inductor L1 current, b) inductor L2 current c) inductor L3 current, d) inductor L4 current, e) summed current after the uncontrolled rectifier

In order to further verify the robustness of the passivity-based control for the IPFC at different inductances, the simulation parameters are adjusted as below: $L_1 = 0.3$ mH, $L_2 = 0.4$ mH, $L_3 = 0.5$ mH and $L_4 = 0.6$ mH. Consequently, the IPFC system also achieves

satisfactory current balancing capability. Figure 6 shows the waveforms of the four-phase inductor currents and the summed current after the uncontrolled rectifier. The ripple of the summed current is much smaller than that of each phase inductor current, which can lower the design difficulty of inductors to a large extent.

Figure 7 shows the partial waveforms of the four inductor currents around time 0.045ms, which shows that their average values are basically equal in any switching period. Therefore, the current passivity-based control can make the four-phase IPFC obtain excellent sharing current performance. When the inductance becomes higher or lower, the peak to peak value of current ripple becomes smaller or larger, however the energy delivered in any switching cycle keeps unchanged.

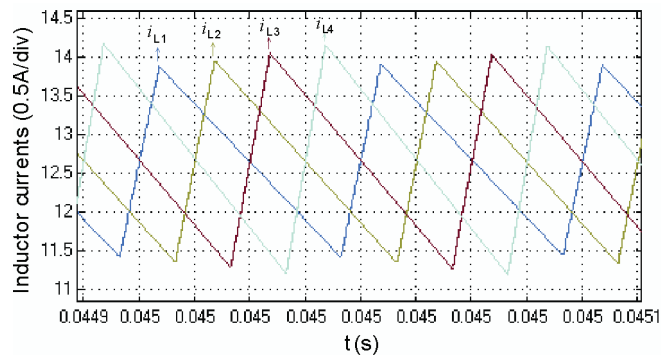


Fig. 7. Partial waveforms of four-phase inductor currents

When using the traditional dual closed loop PI regulator, it is uneasy to regulate the controlled parameters. For wide load applications, the PFC is deficient to meet large power load and light power load at the same time.

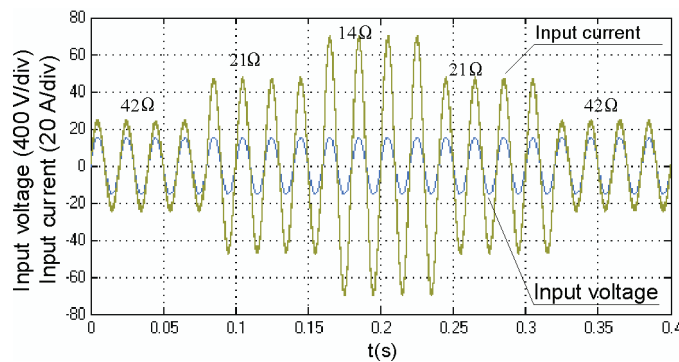


Fig. 8. Waveforms of mains voltage and mains current at different loads

Nevertheless, when using the passivity-based control method, the IPFC is capable of tracking the given mains current and DC output voltage. When the load varies, the dynamic response is fast enough. Waveforms of mains voltage and mains current as well as DC output

voltage at different loads are shown in Figure 8 and Figure 9 respectively, where the load resistance varies from 42 Ω, 21 Ω, 14 Ω, 21 Ω to 42 Ω within interval [0, 0.4 s]. From Figure 8, the THD of mains current are 2.33% when 42 Ω, 1.86% when 21 Ω and 1.46% when 14 Ω.

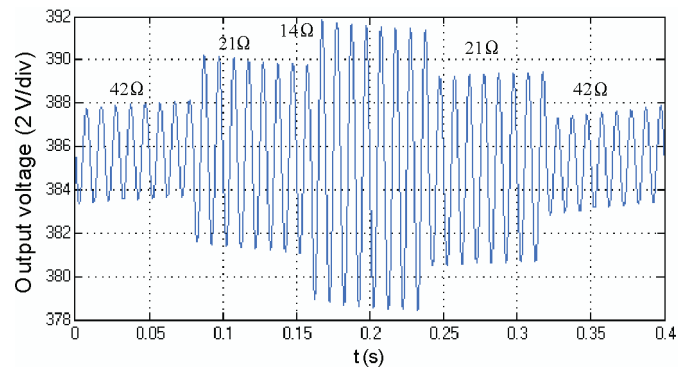


Fig. 9. Waveform of DC output voltage at different loads

From Figure 9, it also can be seen that the DC output voltage can still maintain constant regardless of load variation. Naturally, when the load turns heavier, the output voltage ripple becomes larger. In order to reduce the ripple voltage, it is necessary to increase the electrolysis capacitance or speed up the response of the voltage loop.

If the IPFC system operates in steady state, to increase the injected damping can approximately reduce the THD of mains current and shorten the stabilization time of the DC output voltage.

5. Experiment analysis

The power circuit and control circuit of the four-phase IPFC is established, which is dedicated for large power cabinet air-conditioner. The power circuit is shown in Figure 10, and a TMS320F28335 evaluation board is employed as the kernel control circuit.

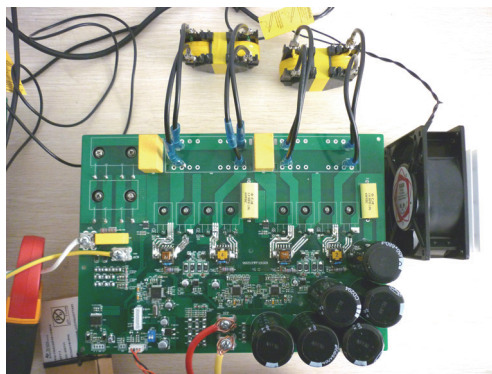


Fig. 10. Power circuit of the four-phase IPFC

The four boost inductors are made of ferrite by using magnet integration technology. One magnetic device includes two integrated inductors, shown in Figure 11. The rated inductance of each inductor is 0.3 mH at frequency 35 kHz and at rated current level. The actual manufacture deviation among different trial inductors is about 10%.

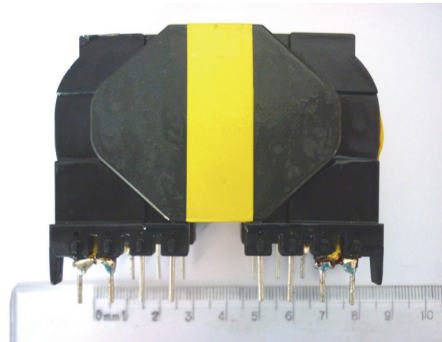


Fig. 11. Two in one magnet integration inductors

The other used power devices include an electrolysis capacitor bank of $6 \times 680 \mu\text{F}/450 \text{ V}$, four fast switching IGBTs of RZH60F7ADPK: 50 A/100°C/600 V, four SiC FRDs of CSD20060D: 20 A/150°C/600 V, two diode rectifiers of D50XB80 connected in parallel and two IGBT drivers of TPS2812. Additionally, four current pulse transformers are used to detect the inductor currents, and the final each inductor current is calculated by current synthesis method. The DC output voltage is sensed by resistor divider, and the load current is sensed via a small shunt resistor.

According to the power requirement of the inverter air-conditioner, the rated mains voltage is 220 V/50 Hz, the mains voltage ranges from 170 V to 265 V/50 Hz, and the expected average DC output voltage is 385 V. The maximum output power of each phase PFC is 3.0 kW. Considering the de-rating coefficient is 13.6% for the four-phase IPFC, then the maximum output power can be over 10.0 kW. Assuming the overall efficiency is 95%, under rated conditions, the maximum RMS value of mains current carried by each phase PFC is 11.5 A. The switching frequency is also set 35 kHz.

TMS320F28335 is selected as the kernel processor, which is used to calculate mains voltage, inductor currents, DC output voltage, load current and the temperature of heat sink. The DSP is also used to perform the passivity-based control and double closed loop PI regulation. It utilizes all the measured electrical quantities and the calculated data to generate the original PWM pulses by comparing the duty ratio signal outputted from current loop with the triangle carrier. The original PWM pulses are interleaved by 1/4 switching period. It is worth noting that the inductances and ESR for inductors are measured in advance.

The passivity-based digital control system for one phase PFC is the same as that shown in Figure 3, which is consistent with that shown in Figure 2.

After hardware and software debugging, the four-phase IPFC is implemented and used to power an inverter air-conditioner. The experimental results show an excellent current sharing performance for the four-phase PFCs at different loads. When at full load, the current error is

less than 5% in terms of RMS value, and mains current ripple is small enough. When at empty load, the average DC output voltage is 385 V. When at the output power of 8.91 kW, the average DC output voltage is 375 V, and the average voltage drop is about 10 V. Figure 12 shows the waveform of the DC output voltage at variable loads, where before 70 seconds, the whole system operates at soft power-on stage and soft start-up phase, at time of about 90 second, a 500 W resistor load is switched on, and at time of about 150 second, the load is switched off, which shows a rapid dynamic respond.

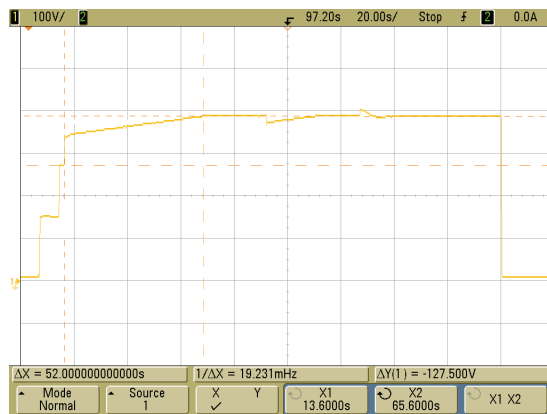


Fig. 12. Waveform of the DC output voltage at variable loads

By changing the room temperature setting, the output load of cabinet air-conditioner can be regulated. When the RMS values of fundamental current are 21.7 A and 40.4 A, Figures 13 and 14 show the measured waveforms of mains voltage and mains current at rated mains voltage respectively.

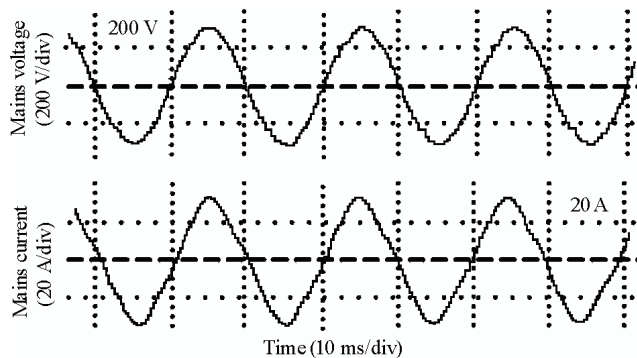


Fig. 13. Waveforms of mains voltage and mains current at load of 4.83 kW

The current error rate of all phase PFCs is normally less than 5%, showing a more satisfactory current sharing effect and power sharing effect. In the first case, the mains power factor is 0.99, and in the second case, the mains power factor is 0.97. When the RMS value of mains current is not larger than 16 A, the produced harmonic currents meet the limits given in IEC61000-3-2. When the RMS value of mains current is larger than 16 A and less than 75 A,

the mains harmonic currents should meet the limits given in IEC61000-3-12, which hasn't gone into effect on a large scale.

When the mains current is below 3.0 A, the IPFC operates in a passive mode, which can improve the overall efficiency. With the increase of the load, the IPFC can smoothly increase the number of phase of IPFC.

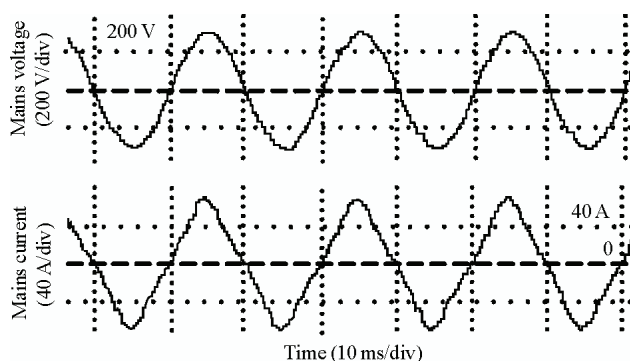


Fig. 14. Waveforms of mains voltage and mains at load of 8.91 kW

6. Conclusions

The EL (Euler-Lagrange) mathematical model of the four-phase interleaved PFC (IPFC) is established in the paper, and the passivity-based controller is also designed using damping injection. Then the four-phase IPFC with the passivity-based control is completely simulated by means of MATLAB/SIMULINK and implemented in a digital way by using TMS320F28335. It is proved that the above passivity-based control strategy can bring about fast tracking effect on the given inductor currents and DC output voltage, leading to a satisfactory power factor correction and stable DC output voltage. Fast tracking capability is very helpful to obtain an excellent current sharing among different phase PFCs for an IPFC. Even when the main device parameters for each phase PFC are greatly different from each other, the IPFC can distribute evenly the same output power among them due to the direct power control. It is also stated that the passivity-based control of the IPFC can be digitally implemented easily and make up for some shortcomings of the exiting control strategies for IPFCs. An experimentation prototype of passivity controlled four-phase IPFC is developed for cabinet inverter air conditioner, the simulated and experimental results proves the passivity-based four-phase IPFC. It is not difficult to say that the passivity-based control is one of considerable alternatives for high power IPFC with the advantage of rapid response performance.

Acknowledgment

The authors would like to thank the National Natural Science Foundation of China (Grant No. 60934005)

References

- [1] Pinheiro J.R., Gründling H.A., Vidor D.L.R., Baggio J.E., *Control strategy of an interleaved BOOST power factor correction converter [J]*. Power Electronics Specialists Conference PESC 99, 30th Annual IEEE, pp. 137-142 (1999).

- [2] Erickson R.W., Maksimovic D., *Fundamentals of power electronics [M]*. 2nd ed. New York: Springer Verlag (2000).
- [3] Nussbaumer T., Kolar J.W., *Design guidelines for interleaved single-phase boost PFC circuits[J]*. IEEE Trans. on Power Electronics 56(7): 2559-2573 (2009).
- [4] Venkataramanan G., Divan D.M., *Discrete time integral sliding mode control for discrete pulse modulated converters*. 21st Annual IEEE Power Electronics Specialists Conference, PESC'90 Record, pp: 67-73 (1990).
- [5] Liu Jin-kun, Sun Fu-chun, *Research and development on theory and algorithms of sliding mode control[J]*. Control Theory and Applications 24(3): 407-418 (2007) (in Chinese).
- [6] Zhang Li, Qiu Shui-sheng, *Analysis and experimental study of sliding mode control inverter[J]*. Proceedings of the CSEE 26(3): 59-63 (2006) (in Chinese).
- [7] Wang Jiu-he, Li Hua-de, Wang Li-ming, *Direct power control system of three phase boost type PWM rectifiers[J]*. Proceedings of the CSEE 26(18): 54-60 (2006) (in Chinese).
- [8] Qiao Shu-tong, Jiang Jian-guo, *Output error passivity control of three-phase boost-type PWM rectifiers[J]*. Transactions of China Electro-technical Society 22(2): 68-73 (2007) (in Chinese).
- [9] Sira-Ramirez H., Perez-Moreno R.A., Ortega R. et al., *Passivity-based controllers for the stabilization of DC to DC power converters [J]*. Automatica 33(4): 499-513 (1997).
- [10] Qiao Shu-tong, Wu Xiao-jie, Jiang Jian-guo, *Application of Passivity-based Sliding Mode Control in DC/DC Converters [J]*. Transactions of China Electro-technical Society 18(4): 41-45 (2003) (in Chinese).
- [11] Wu Lei-tao, Yang Zhao-hua, Xu Bu-gong, *Investigation of Passivity-Based Control of DC/DC Converter[J]*. Transactions of China Electro-technical Society 19(4): 66-69 (2004) (in Chinese).
- [12] Xue Hua, Jiang Jian-guo, *Study on adaptive passivity-based control strategies of shunt active filters [J]*. Proceedings of the CSEE 27(25): 114-118 (2007) (in Chinese).
- [13] Zhang Zhen-huan, Liu Hui-jin, Li Qiong-lin et al., *A novel passivity-based control algorithm for single-phase active power filter using Euler-Lagrange model[J]*. Proceedings of the CSEE 28(9): 37-44 (2008) (in Chinese).
- [14] Wang Jiu-he, *Passivity-based control theory and its application [M]*. Beijing: Publishing House of Electronics Industry (2010) (in Chinese).
- [15] Olmos-López A., Guerrero G., Arau J., *Passivity-based control for current sharing in PFC interleaved boost converters[J]*. Applied Power Electronics Conference and Exposition (APEC), 2011 Twenty-Sixth Annual IEEE pp. 37-44 (2011).
- [16] Rosa A.H.R., Junior S.I.S., Morais L.M.F., *Passivity-based control of PFC boost converter with high-level programming[J]*. Power Electronics Conference(COBEP), pp.: 801-806 (2011).
- [17] Zhaohua Yang, Leitao Wu. *A new passivity-based control method and simulation for DC/DC converter[J]*. Intelligent Control and Automation, 2004. WCICA 2004, Fifth world Congress on 6: 5582-5585 (2004).
- [18] Zuohua Xu, Jiuhe Wang, Pengfei Wang, *Passivity-based control of induction motor based on euler-lagrange (EL) model with flexible damping[J]*. Electrical Machines and Systems pp.: 48-52 (2008).
- [19] Tzann-Shin Lee, *Lagrangian modeling and passivity-based control of three-phase AC/DC voltage-source converters[J]*. Industrial Electronics 51(4): 892-902 (2004).
- [20] Sira-Ramirez H., Ortega R., *Passivity-based controllers for the stabilization of DC-to-DC power converters[J]*. Decision and Control, 1995, Proceedings of the 34th IEEE 4: 3471-3476 (1995).